JOURNAL OF AIRCRAFT
Vol. 44, No. 6, November–December 2007

# Engineering Notes

*ENGINEERING NOTES are short manuscripts describing new developments or important results of a preliminary nature. These Notes should not exceed 2500 words (where a figure or table counts as 200 words). Following informal review by the Editors, they may be published within a few months of the date of receipt. Style requirements are the same as for regular contributions (see inside back cover).*

## Reduced-Order-Model-Based Flutter Analysis at High Angle of Attack

Weiwei Zhang* and Zhengyin Ye†
*Northwestern Polytechnical University, 710072 Xi'an, People's Republic of China*

DOI: 10.2514/1.32285

### Introduction

CONFIGURATIONS with a highly flexible delta wing are considered for the next generation of unmanned air vehicles (UAV). Delta wing flowfield is dominated by vortical structures at high angle of attack, the most prominent is called leading-edge vortex. Ye and Zhao [1] used a nonlinear lifting line method to compute the aerodynamic loads of the delta wing at high angle of attack. With the development of computer technology, computational fluid dynamics (CFD) technique has been used in the simulation of delta wing-induced vortical flow. The study [2] shows that the Reynolds number affects primary vortex slightly, and so Euler codes can be employed to simulate the vortex and aerodynamic loads; the shortness is that it cannot simulate the secondary vortex caused by the effect of viscosity. The CFD and computational structural dynamics (CSD) direct coupling method has been used in aeroelastic analysis of delta wing. Gordnier et al. [3,4] coupled Euler/Navier–Stokes codes and nonlinear plant element to study the buffet problem of the flexible delta wing at high angle of attack. The CFD and CSD direct coupling method [5–7] has also been used in the nonlinear flutter simulation of delta wing at small angle of attack (<5 deg).

The limitation of the direct aeroelastic simulation method is the high cost of the computational time. To solve the contradiction between computational efficiency and computational quality, many researchers turn to CFD-based unsteady aerodynamic reduced-order modeling (ROM) to improve the aeroelastic computational efficiency in the last decade. Dowell and Hall [8], Lucia et al. [9], and Zhang and Ye [10] present some overviews of ROM and its applications on nonlinear aeroelastic research. There are two kinds of methods for ROM of unsteady aerodynamic loads at the present time. The one is the proper orthogonal decomposition (POD) based reduced-order modeling method, the other is aerodynamic modeling based on structural modes by using identification technology. The second method is used in this work. Zhang [11] compared the efficiency between the ROM-based method and the CFD direct simulation method. Efficiency can be improved by $1 \sim 2$ orders with accuracy still retained by ROM-based method. Zhang used CFD-based ROM to perform aeroservoelastic analysis [12] and transonic flutter suppression by active control [13].

Received 22 May 2007; revision received 29 July 2007; accepted for publication 31 July 2007. 

*Ph.D., College of Aeronautics, National Key Laboratory of Aerodynamic Design and Research; aeroelastic@nwpu.edu.cn. Corresponding Author. Member AIAA.

†Professor, College of Aeronautics, National Key Laboratory of Aerodynamic Design and Research; yezy@nwpu.edu.cn. Chief of the Department.

### ROM-Based Flutter Analysis

A finite volume-based unstructured Euler solver is used for unsteady flow computations. It is suitable for moving bodies using an arbitrary Lagrangian–Eulerian (ALE) formulation and adding a dynamically deforming mesh algorithm. Spatial discretization is accomplished by cell-centered finite volume formulation using a center scheme or AUSM + up scheme. A second-order accurate, full implicit scheme is used to integrate the equations in time domain and a fourth Runge–Kutta time marching method is used in the pseudo time step. Local time stepping and implicit residual smoothing accelerates its convergence. The validation with experiments for static and unsteady aerodynamic coefficients has been documented previously. More detailed processes can be found in [14].

CFD-based ROM is used for the flutter analysis. The identification technique is used to construct the reduced-order model based on the structural modes. The time cost of the ROM-based flutter analysis method is mainly used on training the model. Only one process of model training is needed for one angle of attack.

Because the unsteady loads are computed in discrete domain, the input–output difference model is chosen for the multi-input/multi-output (MIMO) system, which is shown in Eq. (1):

$$\boldsymbol{f}_a(k) = \sum_{i=1}^{na} \boldsymbol{A}_i \boldsymbol{f}_a(k-i) + \sum_{i=1}^{nb-1} \boldsymbol{B}_i \boldsymbol{\xi}(k-i) \tag{1}$$

where $\boldsymbol{f}_a$ is the vector of system outputs (generalized aerodynamic force coefficient vector ) and $\boldsymbol{\xi}$ is the vector of system inputs (generalized structural coordinate vector). $\boldsymbol{A}_i$ and $\boldsymbol{B}_i$ are the constant coefficients to be estimated. The model orders $na$ and $nb$ are determined by the user. Multistep input is employed due to its ease of implementation and broad frequency content. The least squares (LS) method is used to estimate the unknown model parameters. To make the data have a zero mean, the data need to remove the constant levels before it is estimated.

To derive the state-space form for aeroelastic analysis, we define a state vector $\boldsymbol{x}_a(k)$, consisting of $(na + nb - 1)$ vector states as follows:

$$\boldsymbol{x}_a(k) = [\boldsymbol{f}_a(k-1), \ldots, \boldsymbol{f}_a(k-na), \boldsymbol{\xi}(k-1), \ldots, \boldsymbol{\xi}(k-nb+1)]^T \tag{2}$$

The state-space form for the discrete-time aerodynamic model is as follows:

$$\begin{cases} \boldsymbol{x}_a(k+1) = \tilde{\boldsymbol{A}}_a \boldsymbol{x}_a(k) + \tilde{\boldsymbol{B}}_a \boldsymbol{\xi}(k) \\ \boldsymbol{f}_a(k) = \tilde{\boldsymbol{C}}_a \boldsymbol{x}_a(k) + \tilde{\boldsymbol{D}}_a \boldsymbol{\xi}(k) \end{cases} \tag{3}$$

where

$$\tilde{\boldsymbol{A}}_a = \begin{bmatrix} \boldsymbol{A}_1 & \boldsymbol{A}_2 & \cdots & \boldsymbol{A}_{na-1} & \boldsymbol{A}_{na} & \boldsymbol{B}_1 & \boldsymbol{B}_2 & \cdots & \boldsymbol{B}_{nb-2} & \boldsymbol{B}_{nb-1} \\ \boldsymbol{I} & \boldsymbol{0} & \cdots & \boldsymbol{0} & \boldsymbol{0} & \boldsymbol{0} & \boldsymbol{0} & \cdots & \boldsymbol{0} & \boldsymbol{0} \\ \vdots & \boldsymbol{I} & \cdots & \boldsymbol{0} & \boldsymbol{0} & \boldsymbol{0} & \boldsymbol{0} & \cdots & \boldsymbol{0} & \boldsymbol{0} \\ \vdots & \vdots & \ddots & \vdots & \vdots & \vdots & \vdots & \ddots & \vdots & \vdots \\ \boldsymbol{0} & \boldsymbol{0} & \cdots & \boldsymbol{I} & \boldsymbol{0} & \boldsymbol{0} & \boldsymbol{0} & \cdots & \boldsymbol{0} & \boldsymbol{0} \\ \boldsymbol{0} & \boldsymbol{0} & \cdots & \boldsymbol{0} & \boldsymbol{0} & \boldsymbol{0} & \boldsymbol{0} & \cdots & \boldsymbol{0} & \boldsymbol{0} \\ \boldsymbol{0} & \boldsymbol{0} & \cdots & \boldsymbol{0} & \boldsymbol{0} & \boldsymbol{I} & \boldsymbol{0} & \cdots & \boldsymbol{0} & \boldsymbol{0} \\ \boldsymbol{0} & \boldsymbol{0} & \cdots & \boldsymbol{0} & \boldsymbol{0} & \boldsymbol{0} & \boldsymbol{I} & \cdots & \boldsymbol{0} & \boldsymbol{0} \\ \vdots & \vdots & \ddots & \vdots & \vdots & \vdots & \vdots & \ddots & \vdots & \vdots \\ \boldsymbol{0} & \boldsymbol{0} & \cdots & \boldsymbol{0} & \boldsymbol{0} & \boldsymbol{0} & \boldsymbol{0} & \cdots & \boldsymbol{I} & \boldsymbol{0} \end{bmatrix}$$

$$\tilde{\boldsymbol{B}}_a = [\tilde{\boldsymbol{B}}_0 \ \boldsymbol{0} \ \boldsymbol{0} \ \cdots \ \boldsymbol{0} \ \boldsymbol{I} \ \boldsymbol{0} \ \boldsymbol{0} \ \cdots \ \boldsymbol{0}]^T$$

$$\tilde{\boldsymbol{C}}_a = [\boldsymbol{A}_1 \ \boldsymbol{A}_2 \ \cdots \ \boldsymbol{A}_{na-1} \ \boldsymbol{A}_{na} \ \boldsymbol{B}_1 \ \boldsymbol{B}_2 \ \cdots \ \boldsymbol{B}_{nb-2} \ \boldsymbol{B}_{nb-1}]$$

$$\tilde{\boldsymbol{D}}_a = [\boldsymbol{B}_0]$$

To couple the structural equations, the discrete-time state-space form is turned into the continue-time form, and the model in state-space form is constructed as shown in Eq. (4):

$$\begin{cases} \dot{\boldsymbol{x}}_a(t) = \boldsymbol{A}_a \boldsymbol{x}_a(t) + \boldsymbol{B}_a \boldsymbol{\xi}(t) \\ \boldsymbol{f}_a(t) = \boldsymbol{C}_a \boldsymbol{x}_a(t) + \boldsymbol{D}_a \boldsymbol{\xi}(t) \end{cases} \tag{4}$$

More detailed processes can be found in [11,13,15].

Equation (5) is the structural motion equations.

$$\boldsymbol{M} \cdot \ddot{\boldsymbol{\xi}} + \boldsymbol{G} \cdot \dot{\boldsymbol{\xi}} + \boldsymbol{K} \cdot \boldsymbol{\xi} = \boldsymbol{F} = q \cdot \boldsymbol{f}_a \tag{5}$$

$\boldsymbol{M}$, $\boldsymbol{G}$, $\boldsymbol{K}$, $\boldsymbol{F}$, and $q$ are the mass matrix, damping matrix, stiffness matrix, generalized forces vector, and dynamic pressure of the free flow. By defining the structural state-vector $\boldsymbol{x}_s = [\xi_1, \ldots, \xi_n, \dot{\xi}_1, \ldots, \dot{\xi}_n]^T$, the structural equations in state-space form and the output equations are as follows:

$$\begin{cases} \dot{\boldsymbol{x}}_s(t) = \boldsymbol{A}_s \cdot \boldsymbol{x}_s(t) + q \cdot \boldsymbol{B}_s \cdot \boldsymbol{f}_a(t) \\ \boldsymbol{\xi}(t) = \boldsymbol{C}_s \cdot \boldsymbol{x}_s(t) + q \cdot \boldsymbol{D}_s \cdot \boldsymbol{f}_a(t) \end{cases} \tag{6}$$

where

$$\boldsymbol{A}_s = \begin{bmatrix} 0 & \boldsymbol{I} \\ -\boldsymbol{M}^{-1}\boldsymbol{K} & -\boldsymbol{M}^{-1}\boldsymbol{G} \end{bmatrix}, \qquad \boldsymbol{B}_s = \begin{bmatrix} 0 \\ \boldsymbol{M}^{-1} \end{bmatrix}$$

$$\boldsymbol{C}_s = [\boldsymbol{I} \ \ 0], \qquad \boldsymbol{D}_s = [0]$$

Define $\boldsymbol{x} = [\boldsymbol{x}_s^T, \boldsymbol{x}_a^T]^T$, coupling the structural state Eq. (6) and aerodynamic state Eq. (4), we get state equations for the aeroelastic system which is as follows:

$$\dot{\boldsymbol{x}} = \boldsymbol{A} \cdot \boldsymbol{x} = \begin{bmatrix} \boldsymbol{A}_s + q \cdot \boldsymbol{B}_s \boldsymbol{D}_a \boldsymbol{C}_s & q \cdot \boldsymbol{B}_s \boldsymbol{C}_a \\ \boldsymbol{B}_a \boldsymbol{C}_s & \boldsymbol{A}_a \end{bmatrix} \cdot \boldsymbol{x} \tag{7}$$

Computing the eigenvalue root loci of the matrix $\boldsymbol{A}$ changing with dynamic pressure, the flutter characteristics of the wing can be analyzed.

## Results and Discussions

A thin, flat plate, cropped delta wing with sweep angle 70 is used to be the example. It is made of aluminum. Finite element analysis package ANSYS was used to analyze the modal properties of the wing model, and the first three eigenmodes are shown in Fig. 1. Figure 2 shows the surface mesh for the flowfield computation and Fig. 3 shows the slice of the body mesh at $x = 0.6$. The Mach number is 0.3. To compute the vortex precisely, the meshes are refined on the upper surface which ensures that the vortex can be captured in detail in the region for $0 < \alpha \leq 20$ deg (Figs. 2 and 3). When $\alpha > 25$ deg, the vortex will break down on the upper surface, finer meshes and a smaller time step are needed to simulate the complex unsteady flow, hence time cost is very high for flutter analysis. The problem for $\alpha > 25$ deg will be studied in the future. The number of the total surface mesh elements is 7416 and the number of the total body mesh elements is 295,166. Figure 4 shows the slices of the pressure at

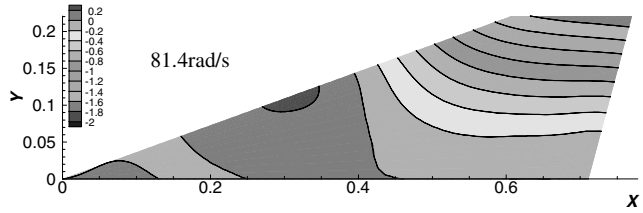


a) 1st mode

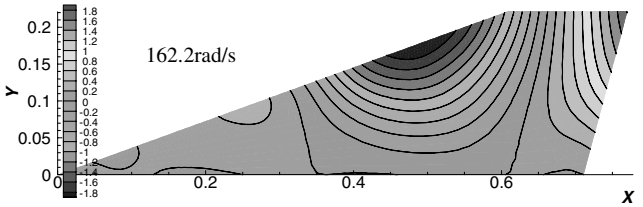


b) 2nd mode

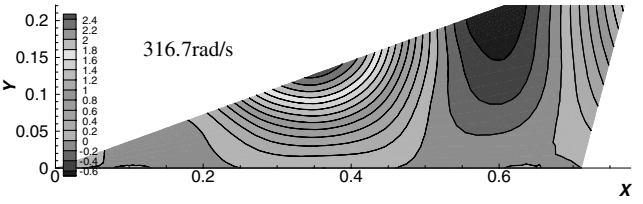


c) 3rd mode

**Fig. 1 Cropped delta wing mode shapes.**

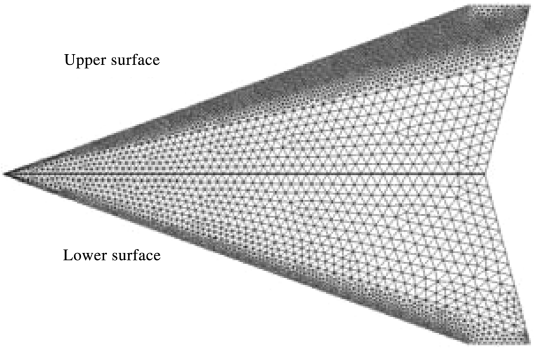


**Fig. 2 Mesh distribution on the upper and lower surfaces.**

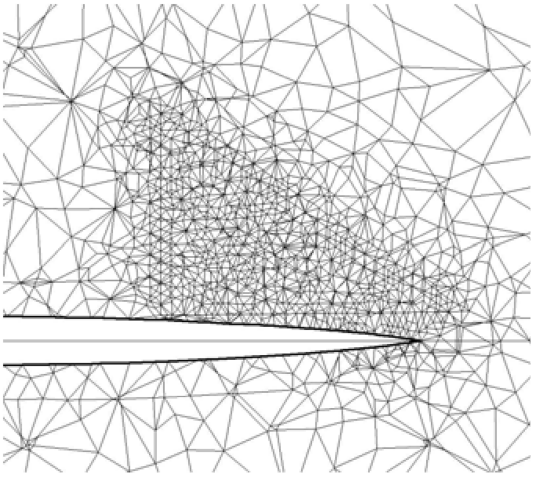

**Fig. 3 Slice of the body meshes at $x = 0.6$.**

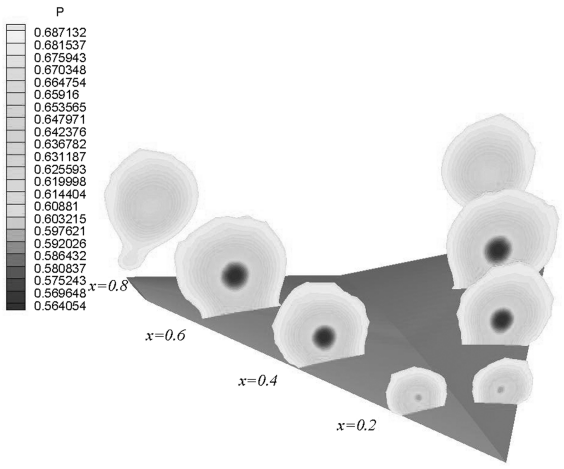


**Fig. 4 Slices of pressure at different locations.**

different locations. It shows that the vortex can be computed precisely by present meshes and codes.

Figure 5 shows the time responses computed by CFD/CSD direct simulation method at different velocities at $\alpha = 20$ deg; the flutter speed is 117.0 m/s and the flutter frequency is 98.8 rad/s. Figure 6 shows the root loci computed by the ROM-based method; the flutter speed is 116.8 m/s and the flutter frequency is 103.9 rad/s. The flutter results (both flutter speed and flutter frequency) by the ROM analysis method agree well with those by the CFD direct simulation method, and so it shows that the unsteady flow due to the wing's small amplitude vibration at high angle of attack before the vortex breakdown can be treated as a linear dynamic problem, and CFD-based linear ROM is suitable for the flutter analysis of the delta wing at high angle of attack. The flutter characteristics of the 70 deg cropped delta wing at different angles of attack are then studied by the ROM-based method. Figure 7 shows the variations of flutter speed and flutter frequency with steady angle of attack. Flutter speed reduces greatly with increasing angle of attack. Flutter speed $\alpha = 20$ deg is reduced by 22% than at $\alpha = 0$ deg.

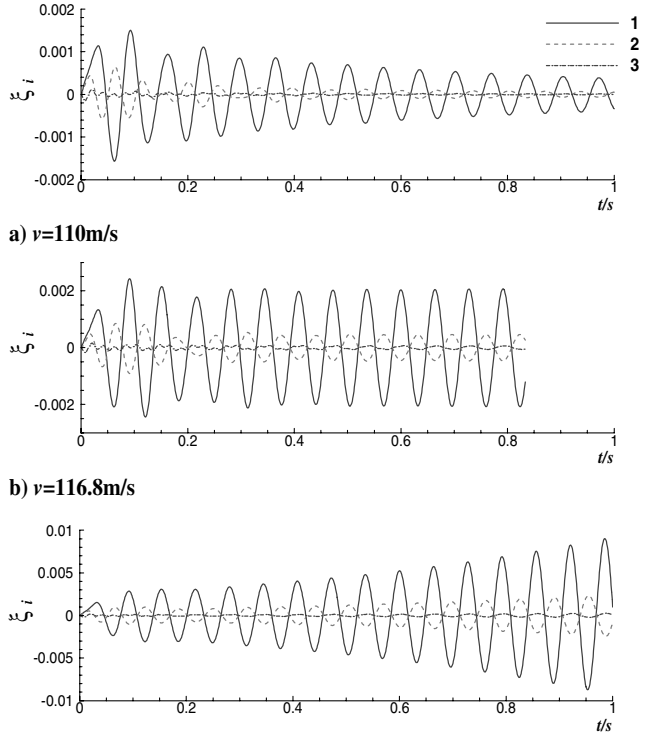


**a) *v*=110m/s**

**b) *v*=116.8m/s**

**c) *v*=120m/s**

**Fig. 5 Time responses of the structural mode coordinates computed by Euler codes.**

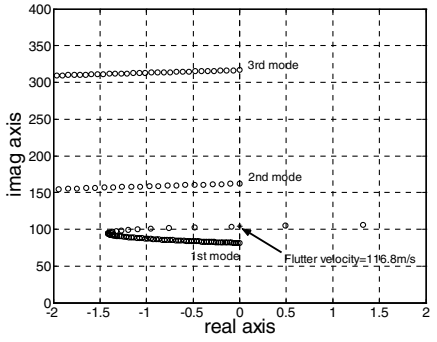


**Fig. 6 Root loci computed by ROM-based method.**

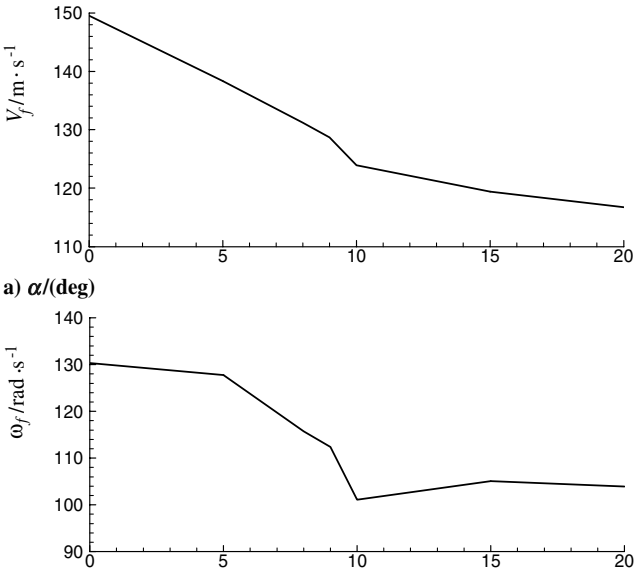


**a) $\alpha$/(deg)**

**b) $\alpha$/(deg)**

**Fig. 7 Flutter characteristics change with $\alpha$.**

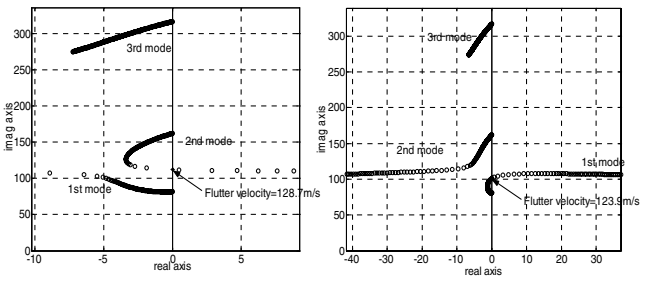


**a) $\alpha = 9$ deg** **b) $\alpha = 10$ deg**

**Fig. 8 Root loci at different steady angles of attack.**

The flutter boundaries have a cusp at about $\alpha = 10$ deg which can be seen in Fig. 7. Comparison of the root loci $\alpha = 9$ deg and $\alpha = 10$ deg will give an explanation of the preceding case (Fig. 8). That is, at this point, the dominate flutter mode changes from the second structural mode to the first structural mode.

## Conclusions

By using CFD-based ROM, the model for flutter analysis of a delta wing at high angle of attack is constructed. The flutter characteristics of a 70 deg cropped delta wing at different angles of attack before the vortex breakdown are studied, and the following conclusions are obtained:

1) Time linear ROM is suitable for studying the unsteady flow due to small amplitude vibration of a delta wing before the vortex

breakdown; it can be employed to delta wing flutter analysis at high angle of attack.

2) Effect of angle of attack on flutter characteristics cannot be neglected. The illustrative example shows that flutter speed greatly reduces with the increasing angles of attack; a 22% decrease of flutter speed at $\alpha = 20$ deg than at $\alpha = 0$ deg has occurred.

3) The flutter mode may change at a certain angle of attack, and then a cusp appears on the flutter boundary.

## Acknowledgments

This work was supported by the National Natural Science Foundation (10432040, 10372085) and Doctorate Creation Foundation of Northwestern Polytechnical University (CX200402). The authors would also like to thank Lingcheng Zhao, Yongnian Yang, and Chen'an Zhang.

## References

[1] Ye, Z., and Zhao, L., "Nonlinear Flutter Analysis of Wings at High Angle of Attack," *Journal of Aircraft*, Vol. 31, No. 4, 1994, pp. 973–974.

[2] Yan, C., Li, T., and Huang, X., "Numerical Simulation of Separation and Vortical Flows on Delta Wing," *Advances in Mechanics*, Vol. 31, No. 1, 2001, pp. 227–244 (in Chinese).

[3] Gordnier, R. E., and Visbal, M., "Computation of the Aeroelastic Response of a Flexible Delta Wing at High Angle of Attack," AIAA Paper 2003-1728, April 2003.

[4] Attar, P. J., Gordnier, R. E., and Visbal, M. R., "Numerical Simulation of the Buffet of a Full Span Delta Wing at High Angle of Attack," AIAA Paper 2006-2075, May 2006.

[5] Gordnier, R. E., "Computation of Limit Cycle of a Delta Wing," AIAA Paper 2002-1411, April 2002.

[6] Attar, P. J., and Gordnier, R. E., "Aeroelastic Prediction of the Limit Cycle Oscillations of a Cropped Delta Wing," AIAA Paper 2005-1915, April 2005.

[7] Hashimoto, A., Furuta, Y., Yag, N., and Nakamura, Y., "Experimental and Numerical Investigation of Delta Wing Flutter in Low Subsonic Flow," AIAA Paper 2006-3215, June 2006.

[8] Dowell, E. H., and Hall, K. C., "Modeling of Fluid Structure Interaction," *Annual Review of Fluid Mechanics*, Vol. 33, 2001, pp. 445–490. doi:10.1146/annurev.fluid.33.1.445

[9] Lucia, D. J., Beran, P. S., and Silva, W. A., "Reduced-Order Modeling: New Approaches for Computational Physics," *Progress in Aerospace Sciences*, Vol. 40, No. 1, 2004, pp. 51–117. doi:10.1016/j.paerosci.2003.12.001

[10] Zhang, W., and Ye, Z., "On Unsteady Aerodynamic Modeling Based on CFD Technique and Its Applications on Aeroelastic Analysis," *Advances in Mechanics* (in Chinese) Vol. 38, No. 1, 2008 (to be published).

[11] Zhang, W., "Efficient Analysis for Aeroelasticity Based on CFD," Ph. D. Dissertation, Northwestern Polytechnical Univ., Xi'an, PRC, 2006.

[12] Zhang, W., Ye, Z., and Zhang, C., "Aeroservoelastic Analysis for Transonic Missile," AIAA Paper 2007-6482, 2007.

[13] Zhang, W., and Ye, Z., "Control Law Design for Transonic Aeroservoelasticity," *Aerospace Science and Technology*, Vol. 11, Nos. 2–3, 2007, pp. 136–145. doi:10.1016/j.ast.2006.12.004

[14] Wang, G., "New Type of Grid Generation Technique Together with the High Efficiency and High Accuracy Scheme Researches for Complex Flow Simulation," Ph.D. Dissertation, Northwestern Polytechnical Univ., Xi'an, PRC, 2005.

[15] Cowan, T. J., Arena, A. S. J., and Gupta, K. K., "Accelerating Computational Fluid Dynamics Based Aeroelastic Predictions Using System Identification," *Journal of Aircraft*, Vol. 38, No. 1, 2001, pp. 81–87.